scientific reports

Check for updates

OPEN

# Preparation of MOF-5 imprinted chromium ferrite and its application in decontaminating metronidazole and penicillin G contaminated water system

Babatunde K. Adeleke[1], Olamide A. Olalekan[2], Adewale Adewuyi[1]✉, Woei Jye Lau[2] & Olalere G. Adeyemi[1]

**Metronidazole (MZ) and penicillin G (PG) are antibiotics frequently detected in aqueous systems as pollutants. Their presence in water systems is a global challenge requiring the development of sustainable solutions for water purification. Therefore, this study synthesized and improved the adsorption performance of chromium ferrite ($CrFe_2O_4$) via incorporation of metal-organic framework (MOF-5) to produce $CrFe_2O_4$@MOF-5 composite. $CrFe_2O_4$@MOF-5 and $CrFe_2O_4$ were characterized using a series of analytical instrument. Both adsorbents exhibited a four-phase mass loss from the thermogravimetric analysis, while the Brunauer-Emmett-Teller (BET) results gave a surface area of 40.94 $m^2\ g^{-1}$ for $CrFe_2O_4$ and 59.76 $m^2\ g^{-1}$ for $CrFe_2O_4$@MOF-5. Interestingly, microscopical images unfolded the surfaces of $CrFe_2O_4$@MOF-5 and $CrFe_2O_4$ to be heterogeneous, while elemental surface mapping confirmed the constituent elements of $CrFe_2O_4$@MOF-5 and $CrFe_2O_4$ to be Cr, Fe, O, C and Zn. $CrFe_2O_4$@MOF-5 exhibited a higher affinity (91.67 mg $g^{-1}$) for PG than $CrFe_2O_4$ (53.82 mg $g^{-1}$). Similarly, the performance of $CrFe_2O_4$@MOF-5 was better (90.24 mg $g^{-1}$) compared to $CrFe_2O_4$ (50.41 mg $g^{-1}$) towards MZ. Both Freundlich and Langmuir isotherm may describe the removal process of MZ and PG by $CrFe_2O_4$@MOF-5 while sorption of MZ and PG by $CrFe_2O_4$ fitted best for Langmuir isotherm in a sorption mechanism involving electrostatic interaction and pore diffusion. The adsorption performance of $CrFe_2O_4$@MOF-5 and its regeneration capacity compared agreeably with most published adsorbents in literature. This current study showed $CrFe_2O_4$@MOF-5 as a potential adsorbent for decontaminating MZ and PG-polluted water systems.**

**Keywords** Adsorbent, Adsorption, Antibiotics, Ferrite, Water purification

The detection of antibiotics as emerging micropollutants in sources of drinking water, tap water and commercially available drinking water is a problem due to its health challenges. Despite the importance associated with the use of antibiotics, their confirmation in drinking water is undesirable because, under certain conditions of temperature, pH and pressure, they may break down into smaller molecules that are injurious to human beings and other lower animals[1–3]. Ingestion of antibiotics from consumption of environmental drinking water may cause disruption of the gut microbiota in human body system[4] including many other metabolic related diseases[5,6]. This has resulted in the emergence of antimicrobial-resistant genes from pathogenic organisms which have developed resistance to known antibiotics; such antibiotics loses their potency posing serious public health concern[7–9]. In fact, ingesting the wrong concentration of pharmaceuticals may have devastating effect[10]. Many research studies have reported several antibiotics in environmental water systems, tap water and commercially available water[11–14] with penicillin G (PG) and metronidazole (MZ) being among the frequently detected antibiotics. The sources of antibiotics (including PG and MZ) in environmental water systems have been linked to aquaculture, domestic and industrial wastes, livestock farming and hospital wastes[15]. Other studies have shown that when consumed, most antibiotics are not fully metabolized by animals and humans

[1]Department of Chemical Sciences, Faculty of Natural Sciences, Redeemer's University, Ede, Osun State, Nigeria. [2]Faculty of Chemical and Energy Engineering, Universiti Teknologi Malaysia, 81310 Skudai, Johor, Malaysia. ✉email: walexy62@yahoo.com

leading to antibiotics being excreted into the environment through feces and urine[16–18] Therefore, this study focused on removing PG and MZ from water systems.

A variety of method has been suggested for eliminating antibiotics from the water system; these methods include membrane technology, photocatalysis, advance oxidation, coagulation, phytoremediation, electrochemical, filtration, adsorption and flocculation[19–26]; however, adsorption stands out due to the possibility of using affordable adsorbents, being selective towards the target antibiotics and the fact that the antibiotics can be reconcentrated after being removed from the aqueous solution. Adsorption is easily applied, controlled and maintained with promising results that can be adapted to large scale application[27–32]. Some adsorbents were reported for removing PG and MZ from water systems[33]. It must be noted that recovering adsorbents from the solution is challenging and may require additional costs to obtain a separation system. Furthermore, the reusability (regeneration) of an adsorbent is very important before being considered to be sustainable and cheap. Even when the adsorption capacity or performance is high, it is desired that the adsorbent is reusable over a long time with high efficiency. One of the focuses of this study is to address this gap by preparing an adsorbent with promising regeneration capacity with high performance over long usage. Consequently, this study proposes using chromium ferrite ($CrFe_2O_4$) due to its prospective properties of magnetism, which allows for easy separation from aqueous solution, small particle size, stability and ease of modification. However, ferrites are known to agglomerate, which is a disadvantage of its use[34]. Therefore, to minimize agglomeration and improve the surface area of $CrFe_2O_4$, this study incorporated $CrFe_2O_4$ in the metal-organic framework (MOF), in this study we proposed MOF-5 to produce $CrFe_2O_4$@MOF-5 composite. Interestingly, recent studies have revealed that MOFs are promising material for water purification[35–38].

A previous study achieved the synthesis of chromium-doped ferrite through a hydrothermal method and applied it in a catalytic removal of tetracycline from aqueous system[39]. Similarly, a recent research work synthesized chromium-doped $Fe_{1.1}Mn_{1.9}O_4$ nanoparticles via the combustion method[40]. The study revealed that the inclusion of chromium in the structure of $Fe_{1.1}Mn_{1.9}O_4$ exhibited a cubic structure, which increased the particle size of $Fe_{1.1}Mn_{1.9}O_4$. Furthermore, chromium-substituted magnesium-zinc ferrite particles were synthesized by thermal synthesis in a self-propagating approach[41]. These studies reported synthetic methods involving the inclusion of chromium in ferrite as a substitution of corresponding metals. In contrast, the current study aims to synthesize $CrFe_2O_4$ via co-precipitation–a simple and less energy-consuming method.

MOF-5 is selected to improve the capacity of $CrFe_2O_4$ because of its well-defined physicochemical properties (pore structure, high thermal stability and large surface area). Moreover, MOFs are excellent materials with a large surface area that can conveniently remove organic substances from water systems[38,42,43]. Although MOF-5 has poor stability in water, some studies have shown that its hydrophobicity improves with the inclusion of nanoparticles[44,45]. Therefore, $CrFe_2O_4$@MOF-5 composite would be an enhanced water-stable adsorbent for removing PG and MZ from water systems. Interestingly, MOF-5 can be easily prepared at room temperature without requiring addition cost for prolong energy supply. Furthermore, the chemicals required for the preparation of MOF and $CrFe_2O_4$ are readily available and affordable. Therefore, combining the magnetic property of $CrFe_2O_4$ and large surface area and pore structure of MOF-5 gives $CrFe_2O_4$@MOF-5 an advantage of enhanced adsorption performance and easy separation from solution after water purification. Currently, there is no published study on the synthesis of $CrFe_2O_4$@MOF-5 for removing PG and MZ from water. Consequently, this study aims to achieve this by comparing the capacities of $CrFe_2O_4$ and $CrFe_2O_4$@MOF-5 for removing PG and MZ from the water system.

## Experimental

### Materials

NaOH, chromium chloride ($CrCl_3$), zinc acetate dihydrate $(CH_3COO)_2Zn.2H_2O$), methanol, terephthalic acid ($C_8H_6O_4$), hydrochloric acid (HCl), oleic acid ($C_{18}H_{34}O_2$), metronidazole (MZ), penicillin G (PG), triethylamine ($C_6H_{15}N$) and ferric chloride ($FeCl_3$) were obtained at Aldrich Chemical, England.

### Synthesis of $CrFe_2O_4$ particles

The synthesis of $CrFe_2O_4$ particles involved stirring chemical solutions containing $CrCl_3$ (0.2 M), $C_{18}H_{34}O_2$ (10 mL) and $FeCl_3$ (0.4 M) in a clean beaker (500 mL) for 1 h maintaning a temperature of 70 °C. Solution of NaOH (2 M) was dropwise added to the reacting solution until black precipitates were formed while stirring at 70 °C for another 1 h. The temperature was reduced to 30 °C and paper-filtered while rising with deionized $H_2O$ and making sure that filtrate is neutral to litmus paper. $CrFe_2O_4$ precipitates produced were dried in the oven (105 °C) for 3 h before being passed onto the furnace and temperature maintained at 550 °C and 18 h. The synthesis is described in Fig. 1.

### Synthesis of MOF-5

Solutions of $(CH_3COO)_2Zn.2H_2O$ (7.24 mmol), $C_8H_6O_4$ (4.10 mmol) and $C_6H_{15}N$ (28.00 mL) were stirred continuously at 30 °C for 24 h in a 500-mL synthesis flask to form a white coloured precipitate which was paper-filtered and rinsed with deionized $H_2O$ until free of acid and alkali. The white product was dried in the oven for 2 h at 70 °C as described in Fig. 2.

### Synthesis of $CrFe_2O_4$@MOF-5 composite

A 2.50 g of MOF-5 dissolved in 50.00 mL $C_6H_{15}N$ was refluxed for 1 h at 70 °C. Furthermore, 2.50 g of $CrFe_2O_4$ particles was poured into the refluxing MOF-5 solution and further refluxed for 2 h. The temperature was gradually reduced to 30 °C, paper-filtered, and rinsed firstly in $C_6H_{15}N$ and then subsequently rinsed many times using deionized $H_2O$ to make it alkali-free. The $CrFe_2O_4$@MOF-5 synthesized was dried overnight maintaining a 70 °C temperature in the oven as shown in Fig. 3.

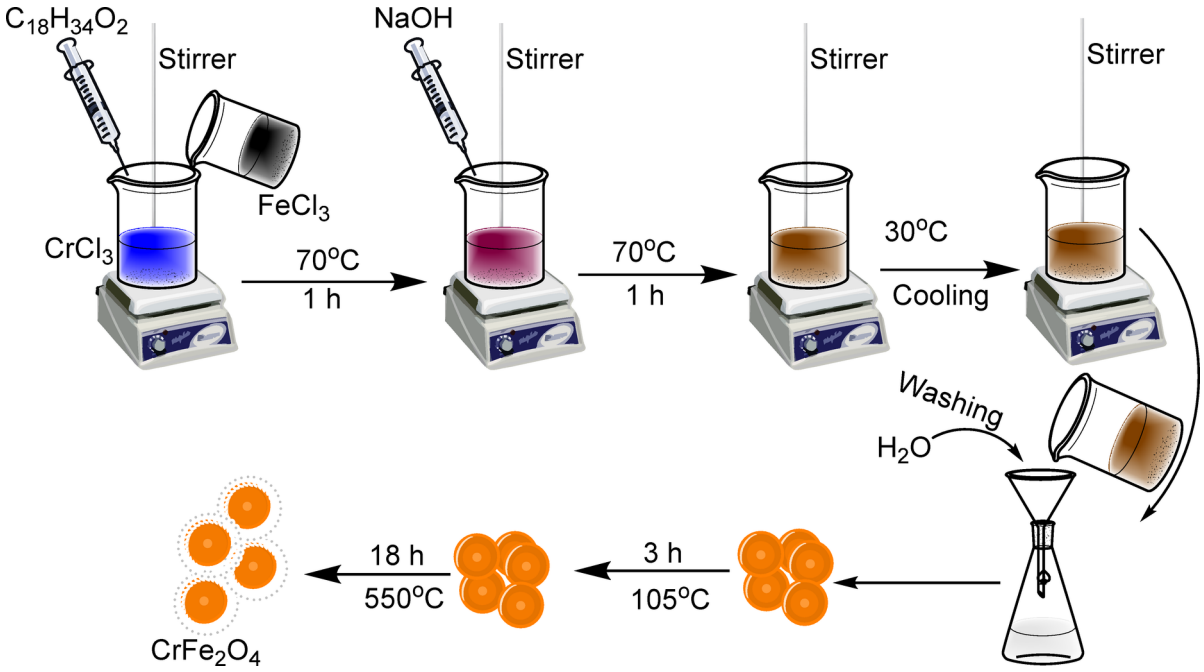


**Fig. 1**. Synthesis of $CrFe_2O_4$.

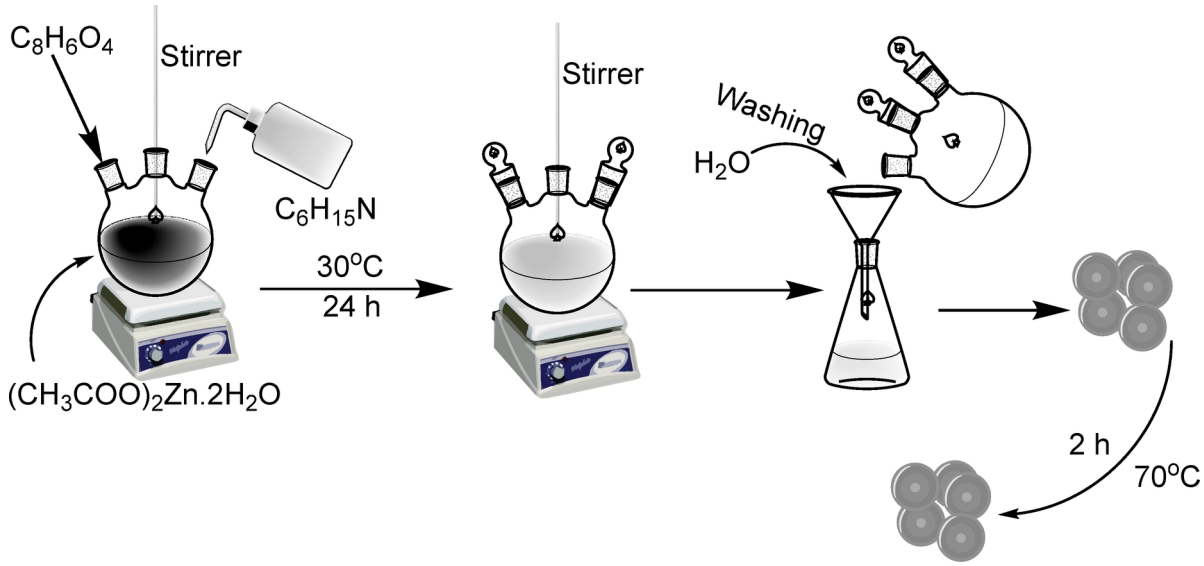


**Fig. 2**. Synthesis of MOF-5.

## Characterisation of $CrFe_2O_4$ and $CrFe_2O_4$@MOF-5

The resulting $CrFe_2O_4$ and $CrFe_2O_4$@MOF-5 were subjected to infrared (FTIR) measurement to determine functional group composition with measurement read from 400 to 4500 $cm^{-1}$. Thermal stability of the nanomaterials was estimated using the TA instrument (TGA Q500-V20) under nitrogen flow. The diffraction pattern on exposure to X-ray (XRD analysis) was measured from 5 to 90 degrees (2θ) using a Panalytical Empyrean diffractometer with the filtered Cu Kβ radiation worked at 40 kV and 40 mA. The surface property was viewed with scanning electron microscopy (TM 3000), enhanced by energy-dispersive X-ray spectroscopy (EDX). The surface area of $CrFe_2O_4$ and $CrFe_2O_4$@MOF-5 was confirmed via Brunauer-Emmett-Teller (BET) nitrogen gas adsorption on Micromeritics, TriStar II 3020 version 3.02.

## Batch adsorption study

Aqueous solutions (100 mL) of MZ or PG were contacted with 0.10 g of $CrFe_2O_4$ or $CrFe_2O_4$@MOF-5 at 150 rpm and 303 K in a conical flask for 2 h while withdrawing 2 mL aqueous sample for UV-visible spectrophotometer

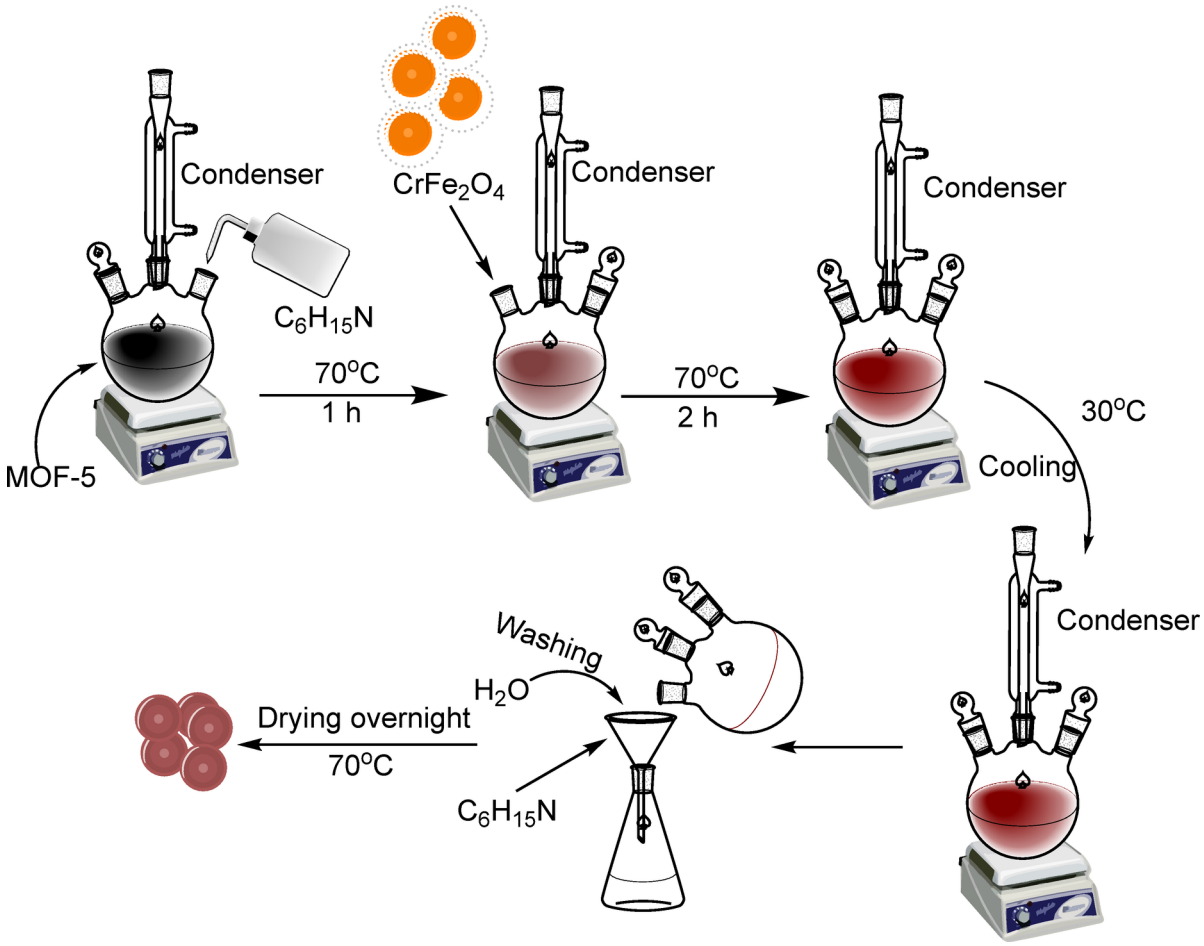


**Fig. 3**. Synthesis of $CrFe_2O_4$@MOF-5 composite.

(Pharo 300-Spectroquant) analysis at interval. The withdrawn $CrFe_2O_4$ or $CrFe_2O_4$@MOF-5-treated antibiotic samples were poured back into the bulk-treated solution immediately after the spectrophotometer reading. The measurements ($\lambda_{max}$) were read at 320 nm for MZ and 283 nm for PG, which are the established maximum absorbance wavelength of the respective antibiotic. The optimum adsorption process parameters for MZ and PG were determined by varying solution concentration (1-100 mg $L^{-1}$), solution pH (1–13), treatment temperature (303–323 K) and weight of adsorbent (0.1–0.5 g). The antibiotic removal efficiency exhibited by $CrFe_2O_4$ or $CrFe_2O_4$@MOF-5 is then calculated from the adsorbent's weight ($m$), test solution's volume ($v$), and initial ($C_o$), time-t ($C_t$), and concentrations in mg $L^{-1}$ at equilibrium ($C_e$). The removal efficiency is determined as adsorption capacity [equilibrium ( $q_e$) and time t ( $q_t$)] in mg $g^{-1}$ and percentage removal (%), which are expressed in Eqs. 1–4[46].

$$q_t = \frac{(C_o - C_t)V}{m} \tag{1}$$

$$q_e = \frac{(C_o - C_e)V}{m} \tag{2}$$

$$Removal = \frac{(C_o - Ct)}{Co} \times 100 \tag{3}$$

$$q_t = \frac{(\%\, removal\ C_o\ V)}{100\ m} \tag{4}$$

## Desorption of antibiotics and regeneration of adsorbents

The antibiotics (MZ or PG) were desorbed from the adsorbents ($CrFe_2O_4$ or $CrFe_2O_4$@MOF-5) to regenerate the adsorbents for reuse via solvent regeneration. Regeneration solvents were selected based on their affinity for MZ, PG and environmental safety. These solvents included deionized water, 0.1 M HCl, 0.1 M NaOH and $CH_3OH$. For the desorption, 0.5 g of $CrFe_2O_4$ or $CrFe_2O_4$@MOF-5 were poured into MZ or PG solution (100 mg $L^{-1}$) in a conical flask and stirred at 150 rpm for 2 h at 30 °C. The $CrFe_2O_4$-MZ/PG or $CrFe_2O_4$@MOF-5-MZ/PG was obtained after passing the test solution through a separation medium (0.22-µm pore size) and

dried for 3 h in the oven at 100 °C. The MZ or PG was desorbed from the adsorbents by shaking $CrFe_2O_4$-MZ/PG or $CrFe_2O_4$@MOF-5-MZ/PG in each of the selected solvents at 150 rpm and 30 °C for 2 h. The test solution was taken at intervals to establish the amount of MZ or PG desorbed by subjecting the taken solution to UV-visible spectrophotometer. The amount of MZ or PG desorbed (%) was calculated by determining the amount of antibiotics desorbed ( $q_d$) and adsorbed ($q_a$) as expressed in Eq. 5 (Adeleke et al., 2024)

$$Desorption = \frac{q_d}{q_a}\ 100 \tag{5}$$

The best desorption performance was obtained using $CH_3OH$. Therefore, a further regeneration study (ten consecutive cycles) was conducted using $CH_3OH$.

## Results and discussion

### Synthesis and characterization of $CrFe_2O_4$ and $CrFe_2O_4$@MOF-5

TGA results of $CrFe_2O_4$, MOF-5 and $CrFe_2O_4$@MOF-5 are presented in Fig. 4a, revealing four mass losses for $CrFe_2O_4$ and $CrFe_2O_4$@MOF-5 as the temperature changes (0 °C to 900ºC) while MOF-5 exhibited five key mass losses. The first mass loss at 30-102 °C in MOF-5, 40-106 °C in the $CrFe_2O_4$ and 45-191ºC in the $CrFe_2O_4$@MOF-5 may be attributed to the loss of adsorbed $H_2O$ and other low molecular weight compounds[47]. The loss in mass from 102 to 211 °C in MOF-5 is attributed to loss of $C_6H_{15}N$ (triethylamine) in its structure and early state of forming metal oxide involving the central cordinating zinc metal while loss in mass from 106 to 335 °C in the $CrFe_2O_4$ may be due to the onset formation of metal oxides. Similarly, mass loss from 191 to 480 °C in the $CrFe_2O_4$@MOF-5 may be attributed to metal oxides' onset formation and organic framework decomposition[48]. The mass loss from 211 to 480 °C in MOF-5 is associated to the collapse of the organic framework structure. The mass loss detected at 480-512 °C in MOF-5 was further detected at 335–511 °C in the $CrFe_2O_4$ and 480–511 °C in the $CrFe_2O_4$@MOF-5 was attributed to inter and intramolecular reactions which led to dehydration of hydroxyl groups within the structure of the ferrite and formation of oxide phase[49,50]. Furthermore, the loss suggests the complete breakdown of the organic structure of MOF-5 and $CrFe_2O_4$@MOF-5. The mass loss above 512 °C in MOF-5 and 511ºC in both $CrFe_2O_4$ and $CrFe_2O_4$@MOF-5 was considered a phase change, leading to the formation of metal oxide.

The diffraction pattern for the $CrFe_2O_4$ and $CrFe_2O_4$@MOF-5 showed most intense peak at $2\theta = 34.07°$ while MOF-5 exhibited its most intense peak at peak at $2\theta = 6.16°$ with planes corresponding to (104), (111), (200), (220), (222), (224), (246), (311), (400), (420), (422), (433), (440), (442), (511), (533) and (711). Interestingly, signals such as (200), (222), (246), (422), (442) and (533) starred in the spectra (Fig. 4b), were not detected in the diffraction of $CrFe_2O_4$ but in the MOF-5 and $CrFe_2O_4$@MOF-5 alone. This suggests them to be the signals arising from the MOF-5 structure and at the same time confirming the inclusion of $CrFe_2O_4$ in MOF-5 structure[51–53]. Diffraction patterns of $CrFe_2O_4$ and $CrFe_2O_4$@MOF-5 align appropriately with JCPDS No. 79-1744 04–016 ($CrFe_2O_4$) and JCPDS No. 96-432-6738 (MOF-5).

The surface area by BET showed the surface area of $CrFe_2O_4$ (Fig. 4c), $CrFe_2O_4$@MOF-5 (Fig. 4d) and MOF-5 (Fig. 4e) to be 40.94, 59.76 and 94.39 $m^2\ g^{-1}$, respectively. This suggests an improvement in surface area capacity by including MOF-5 in $CrFe_2O_4$ forming $CrFe_2O_4$@MOF-5. A previous study has shown the BET area of MOF-5 > 260 $m^2\ g^{-1}$ [54]; such a high surface area accredited to MOF-5 must have resulted in the 59.76 $m^2\ g^{-1}$ obtained for $CrFe_2O_4$@MOF-5. Furthermore, the pore volume of $CrFe_2O_4$ increased from 0.158 to 0.266 $cm^2\ g^{-1}$ in the $CrFe_2O_4$@MOF-5 with the pore volume of MOF-5 being 0.092 $cm^3\ g^{-1}$. Similarly, the pore size distribution increased from 15.46 nm in the $CrFe_2O_4$ to 17.81 nm in the $CrFe_2O_4$@MOF-5 while that of MOF-5 is 3.90 nm. These improvements (15.2% increase) suggest better surface functionality of $CrFe_2O_4$@MOF-5 over $CrFe_2O_4$. The spectrum pattern of MOF-5, $CrFe_2O_4$@MOF-5 and $CrFe_2O_4$ is typical of macroporous materials, suggesting a type II BET isotherm pattern (Kajama et al., 2015). The macroporousity of is an indication of large pores that can participate in adsorption of molecules with multilayer adsorption capacity[55]. This suggests that MOF-5, $CrFe_2O_4$@MOF-5 and $CrFe_2O_4$ exhibits potentials that qualifies them as adsorbents for PG and MZ. Furthermore, the macroporousity suggests free drain via gravity indicating easy flow of fluid through $CrFe_2O_4$@MOF-5 and $CrFe_2O_4$, therefore, suggesting less occurrence of clogging or attrition when $CrFe_2O_4$@MOF-5 and $CrFe_2O_4$ are used in the adsorption process. The FTIR spectra of $CrFe_2O_4$@MOF-5 and $CrFe_2O_4$ (Fig. 4f) exhibited similar signals at 3419 $cm^{-1}$ (O-H stretch from adsorbed $H_2O$ molecules), 1618 $cm^{-1}$ (O-H bending), 997 $cm^{-1}$ (O-Fe-O stretch), 663 $cm^{-1}$ (Fe-O stretch) and 396 $cm^{-1}$ (Cr-O stretch). However, additional signals were only found in the $CrFe_2O_4$@MOF-5. Thses include signals at 2251 $cm^{-1}$ (C-O vibration of carbonyl group from MOF-5 ring structure), 1102 $cm^{-1}$ (aromatic ring stretching from MOF-5 structure) and 403 $cm^{-1}$ (Zn-O stretch from MOF-5 ring structure). The EDS (Fig. 4g) signals confirmed Cr, Fe and O in $CrFe_2O_4$@MOF-5 and $CrFe_2O_4$. In addition, C and Zn were only confirmed in the structure of $CrFe_2O_4$@MOF-5 and MOF. Furthermore, Cr was found in MOF-5 because it was coated with Cr via sputtering technique to increase electrical conductivity and the quality of the micrographs.

SEM images revealed a heterogeneous surface with the surface of $CrFe_2O_4$ (Fig. 5a) showing a consistent pattern of particle arrangement with patches. The surface mapping shown in Fig. 5b corroborates the constituent element confirmed by the EDS results. Furthermore, the surface of MOF-5 (Fig. 5c) revealed a homogeneous surface with consistently ordered particles which appers to be flaky having different sizes. The surface elemental mapping of MOF-5 is shown in Fig. 5d **(I-III)**. On the other hand, the surface of $CrFe_2O_4$@MOF-5 (Fig. 5e) showed irregularly sized particles, which are rod and spherically shaped, with the corresponding surface mapping as shown in Fig. 5f.

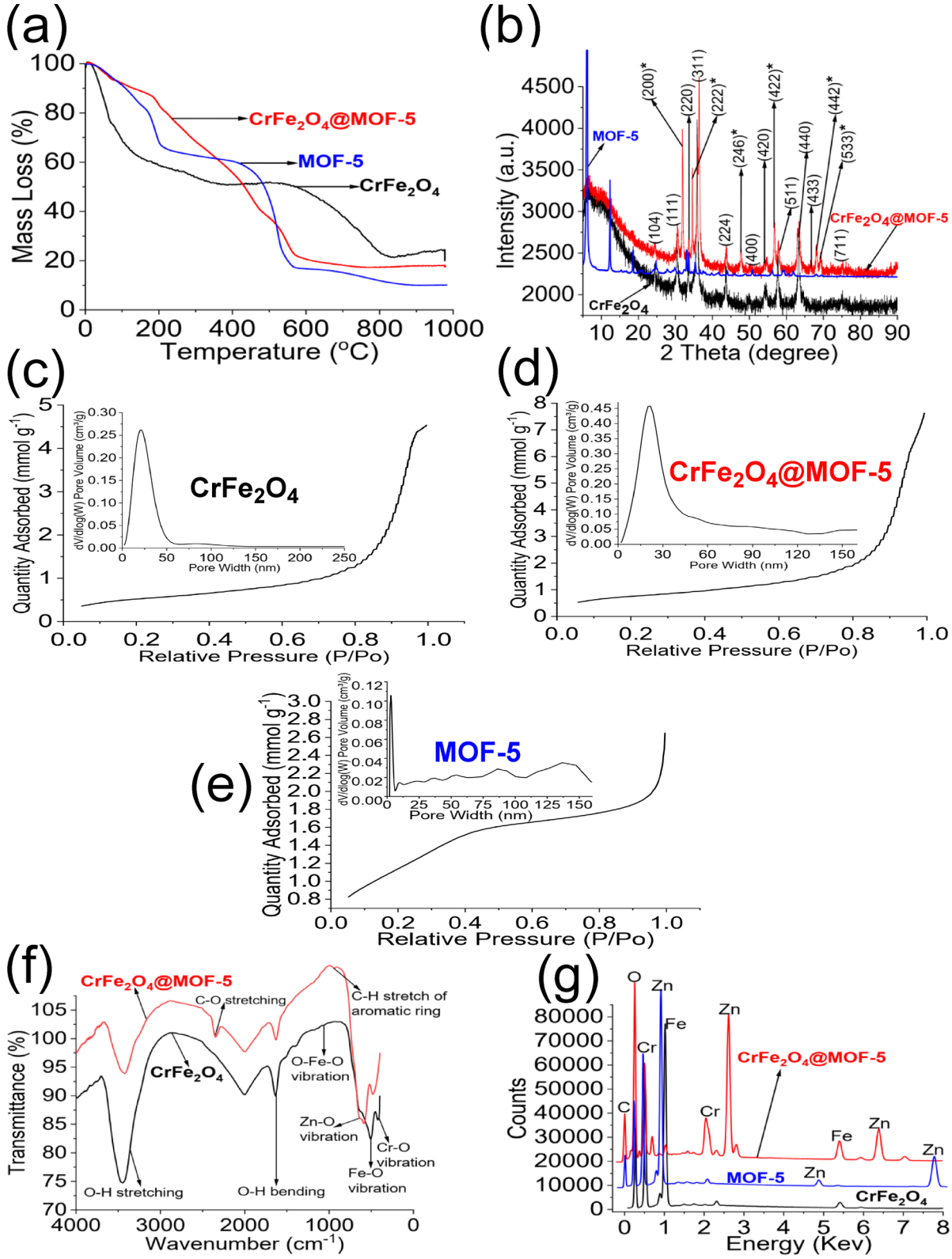


**Fig. 4**. Properties of $CrFe_2O_4$, MOF-5 and $CrFe_2O_4$@MOF-5; (**a**) TGA, (**b**) XRD, (**c**–**e**) BET, (**f**) FTIR spectra and (**g**) EDX.

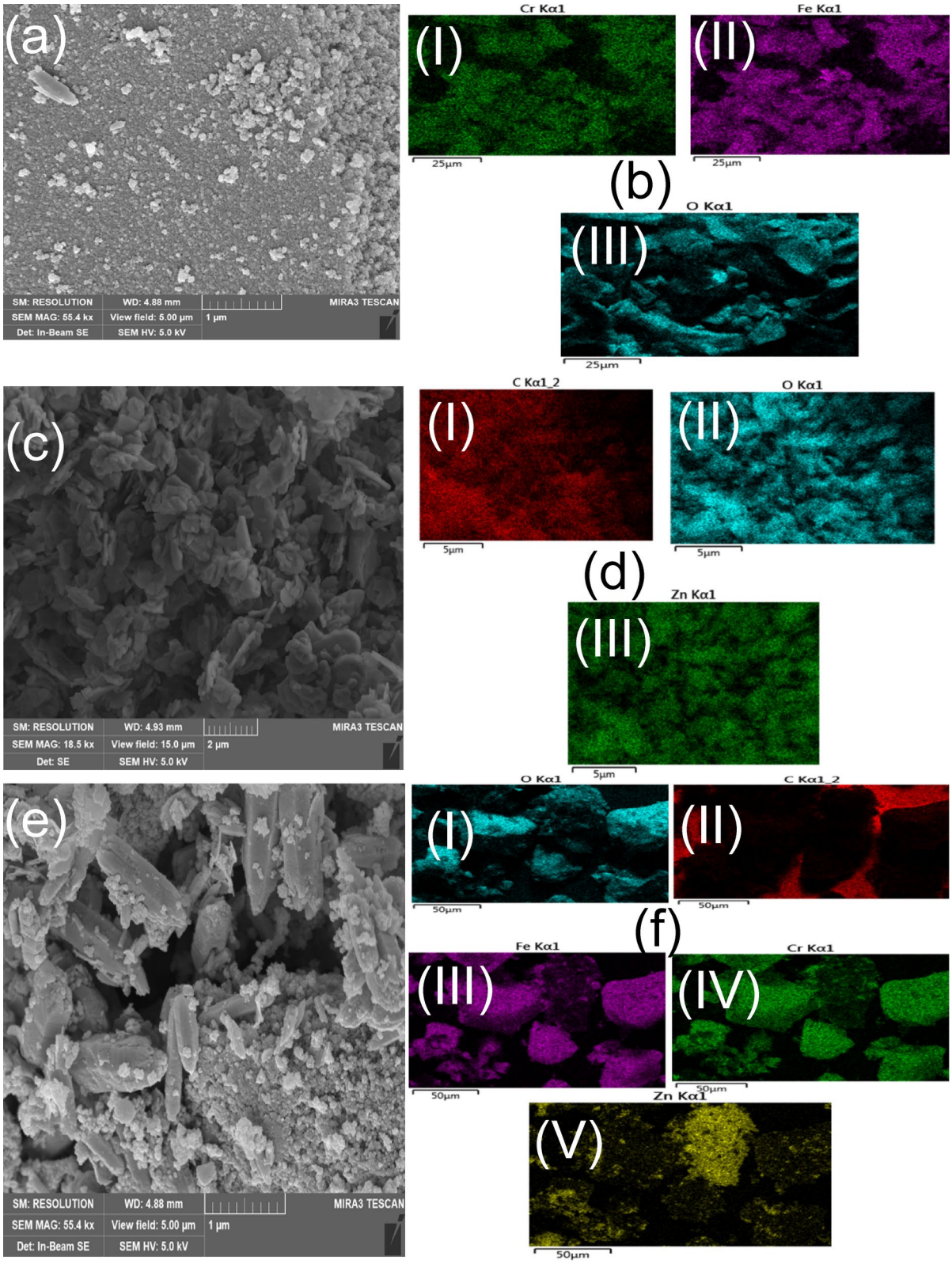


**Fig. 5**. (**a**) SEM image of $CrFe_2O_4$ and its elemental surface mapping (**b** I-III), (**c**) SEM of MOF-5 and its elemental surface mapping (**d** I-III) and (**e**) SEM image of $CrFe_2O_4$@MOF-5 and its elemental surface mapping (**f** I-V).

### Sorption of antibiotics by $CrFe_2O_4$@MOF-5 and $CrFe_2O_4$

The adsorption capacities expressed towards PG by the $CrFe_2O_4$@MOF-5 (Fig. 6a) and $CrFe_2O_4$ (Fig. 6b) and towards MZ by the $CrFe_2O_4$@MOF-5 (Fig. 6c) and $CrFe_2O_4$ (Fig. 6d) demonstrated a steady increase in performance as adsorption treatment time increased. This indicated that the sorption of MZ and PG by $CrFe_2O_4$@MOF-5 and $CrFe_2O_4$ is time dependent. $CrFe_2O_4$@MOF-5 exhibited a higher antibiotic removal capacity (91.67 mg $g^{-1}$) towards PG than $CrFe_2O_4$ (53.82 mg $g^{-1}$). Similarly, the performance of $CrFe_2O_4$@MOF-5 is better (90.24 mg $g^{-1}$) compared to $CrFe_2O_4$ (50.41 mg $g^{-1}$) towards MZ. The enhanced performance exhibited by $CrFe_2O_4$@MOF-5 could be related to its improved surface area capacity. The adsorption capacities of $CrFe_2O_4$@MOF-5 and $CrFe_2O_4$ increased with increased concentration of test solution, which may be due to the higher availability of MZ and PG species in solution for nanomaterials to interact with. The percentage removal exhibited by $CrFe_2O_4$@MOF-5 and $CrFe_2O_4$ towards the antibiotics increased as weight increased.

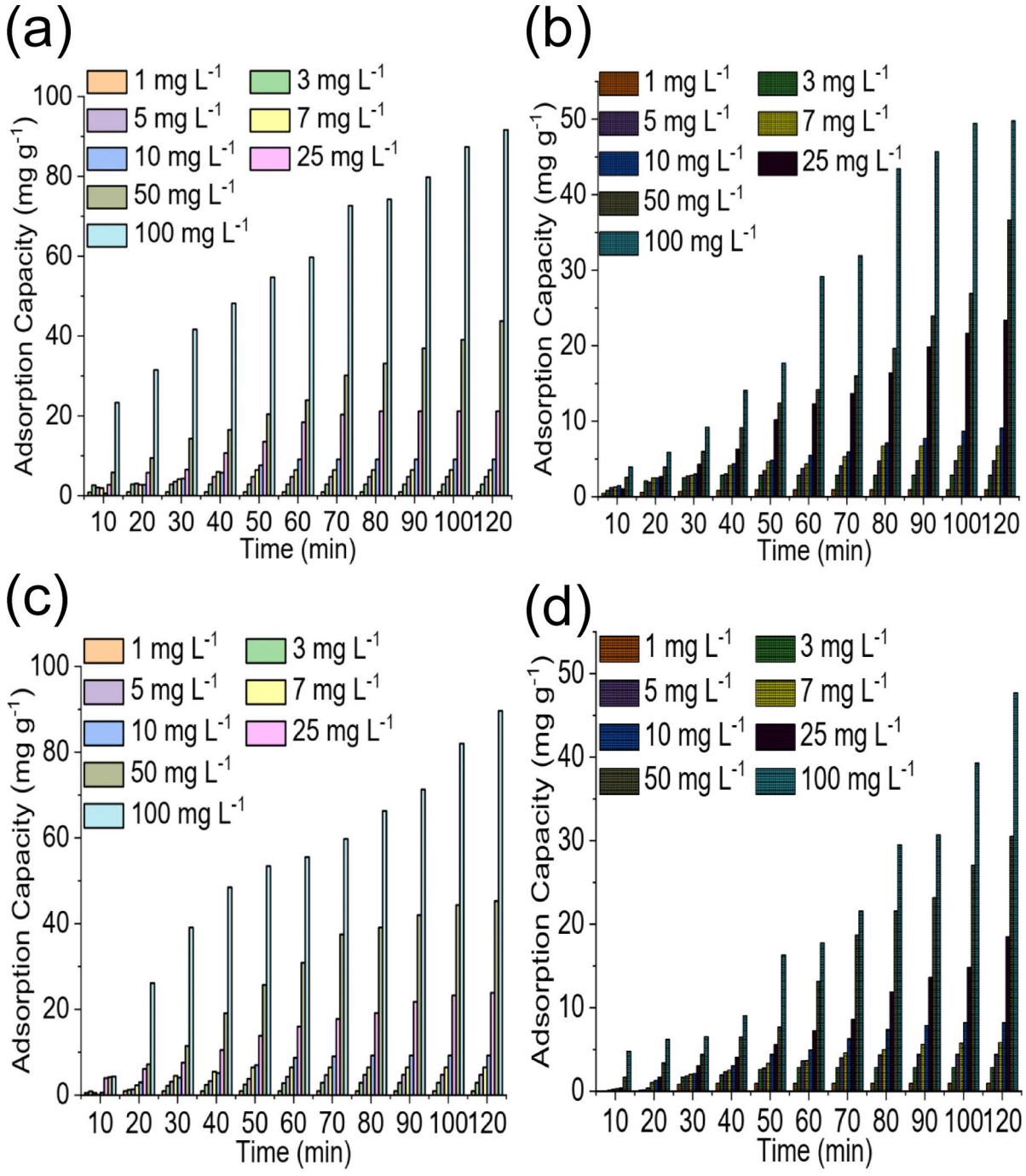


**Fig. 6**. Time dependent adsorption capacities expressed by $CrFe_2O_4$@MOF-5 (**a**) and $CrFe_2O_4$ (**b**) towards PG at varying solution concentrations, and time dependent adsorption capacities expressed by $CrFe_2O_4$@MOF-5 (**c**) and $CrFe_2O_4$ (**d**) towards MZ at varying solution concentrations.

However, on the contrary, the peformance decreased as weight increased (Fig. 7a-d). The observed increase in % removal may be attributed to an increase in available active surface area as weight increased; conversely, the decrease in efficiency of $CrFe_2O_4$@MOF-5 and $CrFe_2O_4$ as their weight was increased may be explained by the mathematical expression in Eq. 4, which showed that as weight increases, the divisor/denominator factor increases leading to a decrease in the performance of $CrFe_2O_4$@MOF-5 and $CrFe_2O_4$.

The molecular structure of PG and MZ is shown in Fig. 8a and b, which show the functional groups for interaction with the surface of the adsorbents. Figure 8c and d revealed that as pH of the test solution is raised towards pH 7, the performance of $CrFe_2O_4$@MOF-5 towards the removal of PG and MZ became better, achieving the highest efficiency for the removing PG and MZ at a test solution pH 7. The performance of $CrFe_2O_4$ towards PG increased with a higher pH value (pH 11 being the best). However, its performance towards MZ is highest at a pH lower than 7 (pH 5 being the best). This observation confirms that solution pH is essential in the performance of adsorbents[47,56]. The surface of $CrFe_2O_4$@MOF-5 remains positively charged as the test solution pH is ≤7, facilitating interaction with the negatively charged surface of MZ/PG in the solution.

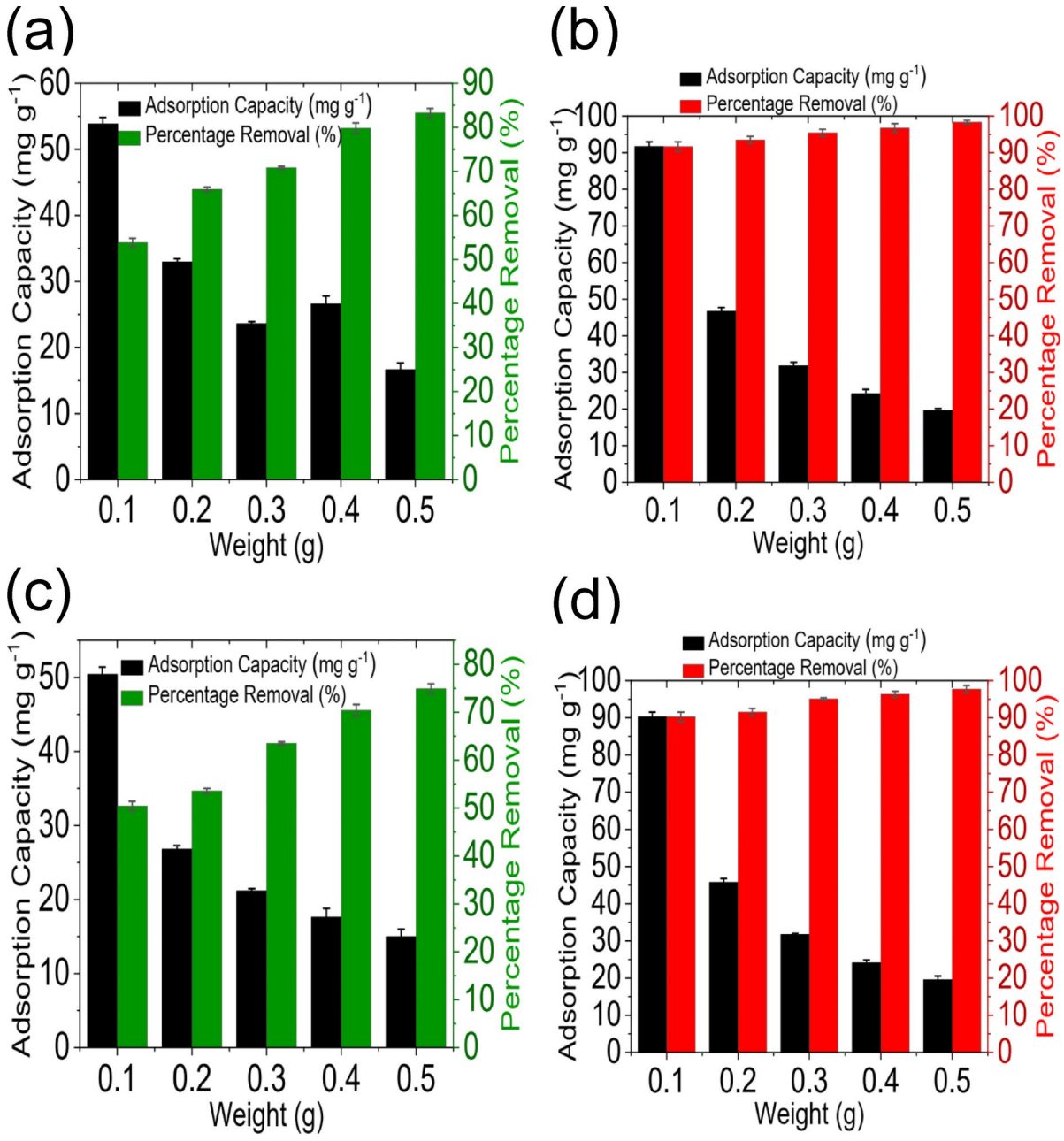


**Fig. 7**. Effect of weight of (**a**) $CrFe_2O_4$ and (**b**) $CrFe_2O_4$@MOF-5 on the adsorption capacity and percentage removal expressed towards PG and effect of weight of (**c**) $CrFe_2O_4$ and (**d**) $CrFe_2O_4$@MOF-5 (**e**) on the adsorption capacity and percentage removal expressed towards MZ (Experimental condition: 100 mg $L^{-1}$ solution).

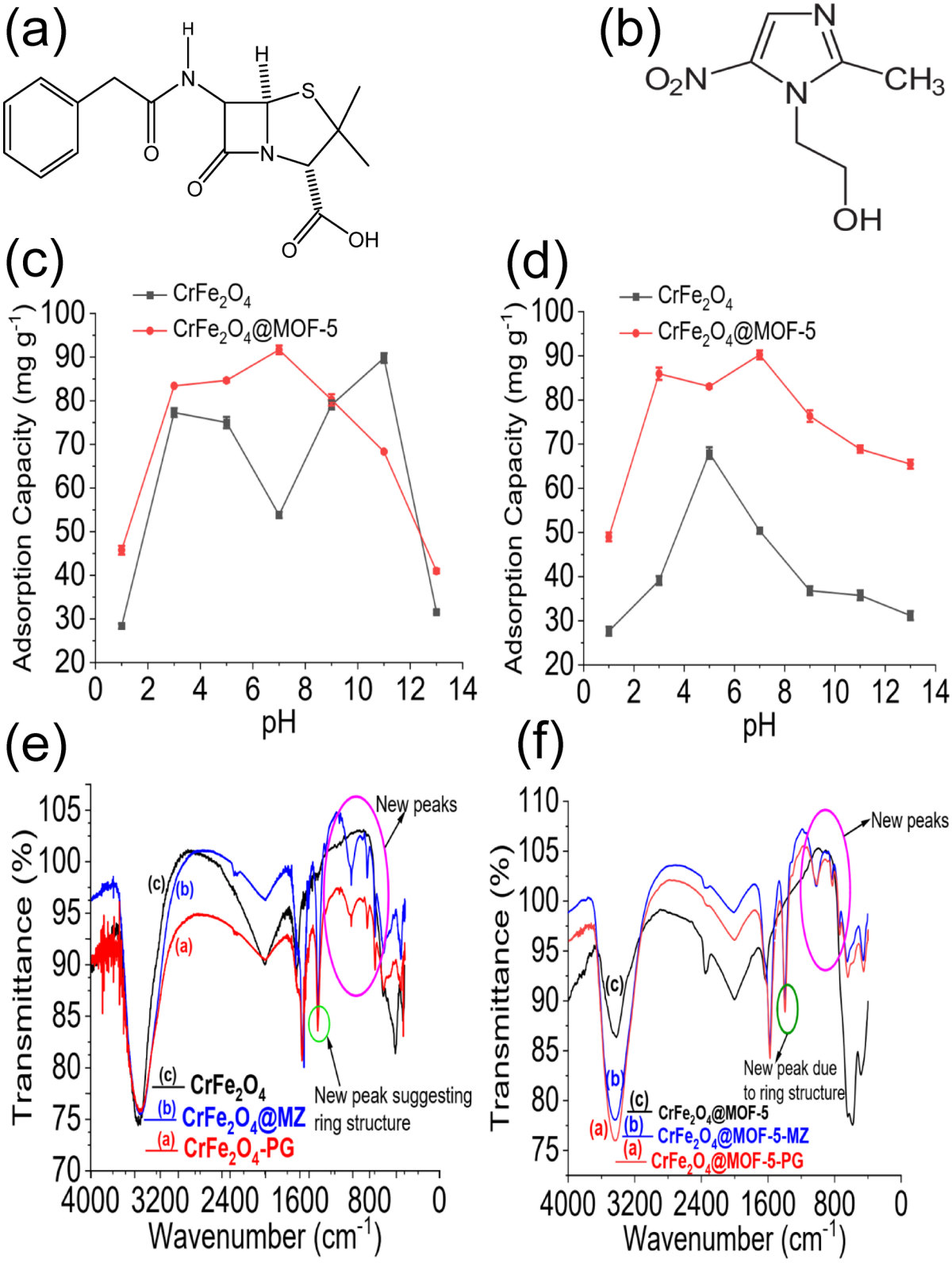


**Fig. 8**. Structures of PG (**a**) and MZ (**b**). Effect of pH change on the removal of PG (**c**) and MZ (**d**) by $CrFe_2O_4$ and $CrFe_2O_4$@MOF-5. Figure 5e: FTIR spectra of pristine $CrFe_2O_4$ (**a**), after adsorbing MZ (**b**) and after adsorbing PG (**c**); Fig. 5f: FTIR spectra of pristine $CrFe_2O_4$@MOF-5 (**a**), after adsorbing MZ (**b**) and after adsorbing PG (**c**).

However, this interaction dropped as pH increased above pH 7, leading to negative charges on the surface of $CrFe_2O_4$@MOF-5, causing a repulsive interaction that reduced the adsorption capacity of $CrFe_2O_4$@MOF-5. On the other hand, $CrFe_2O_4$'s is positively charged as the PG test solution pH becomes ≤ 11, facilitating the attraction of negatively charged PG ions. Regarding MZ, $CrFe_2O_4$'s surface become positively charged as the test solution pH becomes ≤ 5, promoting the removal of MZ. Unfortunately, the adsorption performance is reduced as the solution becomes pH > 5. The FTIR spectra of $CrFe_2O_4$ and $CrFe_2O_4$@MOF-5 before and after adsorption of MZ and PG are shown in Fig. 8e and f. After the removal of MZ and PG from solution, the spectra for the O-H strech became broader suggesting electronic interaction between the surface of the adsorbents and the antibiotics; furthermore, a new peak appeared at 1464–1489 $cm^{-1}$ in $CrFe_2O_4$ and $CrFe_2O_4$@MOF-5 (only after adsorption) which may be attributed to the ring structure of MZ (C = N and C = C streches) and PG (C = C and C-N vibrations). Additional new peaks were seen at 1203, 1005 and 748 $cm^{-1}$ which may be attributed to N = O symmetric streching, C-N and N-H vibrations, respectively. The mechanism of this interaction is shown in Fig. 9a-c, which suggests an electrostatic form of interaction between $CrFe_2O_4$@MOF-5/$CrFe_2O_4$ and MZ/PG. Furthermore, the pore volume and size of $CrFe_2O_4$@MOF-5 and $CrFe_2O_4$ further suggest pore diffusion of MZ and PG within the structure of nanomaterials.

## Process kinetic and isotherm fittings

Data generated during the treatment process were fitted to describe the pseudo-1st and 2nd -order kinetics. The pseudo-1st -order rate constant, $k_1$ ($min^{-1}$) and pseudo-2nd -order rate constant, $k_2$ (g $mg^{-1}$ $min^{-1}$), were determined from the $q_t$ (mg $g^{-1}$), time, $t$ and $q_e$ (mg $g^{-1}$). Expression for the pseudo-1st -order is given as[57]:

$$log\ (q_e - q_t) = \log q_e - \frac{k_1}{2.303} t \tag{6}$$

The plot of ln ($q_e$-$q_t$) against t allowed for the estimation of the $k_1$ values, which were found to be $8.7 \times 10^{-5}$ and 1.97 $min^{-1}$ for $CrFe_2O_4$ and $CrFe_2O_4$@MOF-5, respectively, for the sorption of MZ whereas it was $9.01 \times 10^{-5}$ and $1.8 \times 10^{-4}$ for $CrFe_2O_4$ and $CrFe_2O_4$@MOF-5, respectively for the sorption of PG as shown in Table 1. The $r^2$ value of $CrFe_2O_4$@MOF-5 (0.98) suggests better fitting for the pseudo-1st -order model for the sorption of MZ and PG. The pseudo-2nd -order model may be described as[58]:

$$\frac{t}{q_t} = \frac{1}{k_2\, q_e^2} + \frac{1}{q_e}\, t \tag{7}$$

The plot of $\frac{t}{q_t}$ $v_s$ t gave an expression from which $k_2$ values were determined for the sorption of MZ and PG by the $CrFe_2O_4$ and $CrFe_2O_4$@MOF-5. The values of $k_2$ for the sorption of MZ are 1.42 and 1.97 g $mg^{-1}$ $min^{-1}$, respectively, for the $CrFe_2O_4$ and $CrFe_2O_4$@MOF-5. The values are $1.18 \times 10^{-6}$ and $1.8 \times 10^{-4}$ g $mg^{-1}$ $min^{-1}$, respectively, for the $CrFe_2O_4$ and $CrFe_2O_4$@MOF-5 for the sorption of PG (Table 2). Values of $k_1$ and $k_2$ exhibited by the $CrFe_2O_4$@MOF-5 towards the antibiotics indicate that the sorption process is faster for the $CrFe_2O_4$@MOF-5 than for $CrFe_2O_4$.

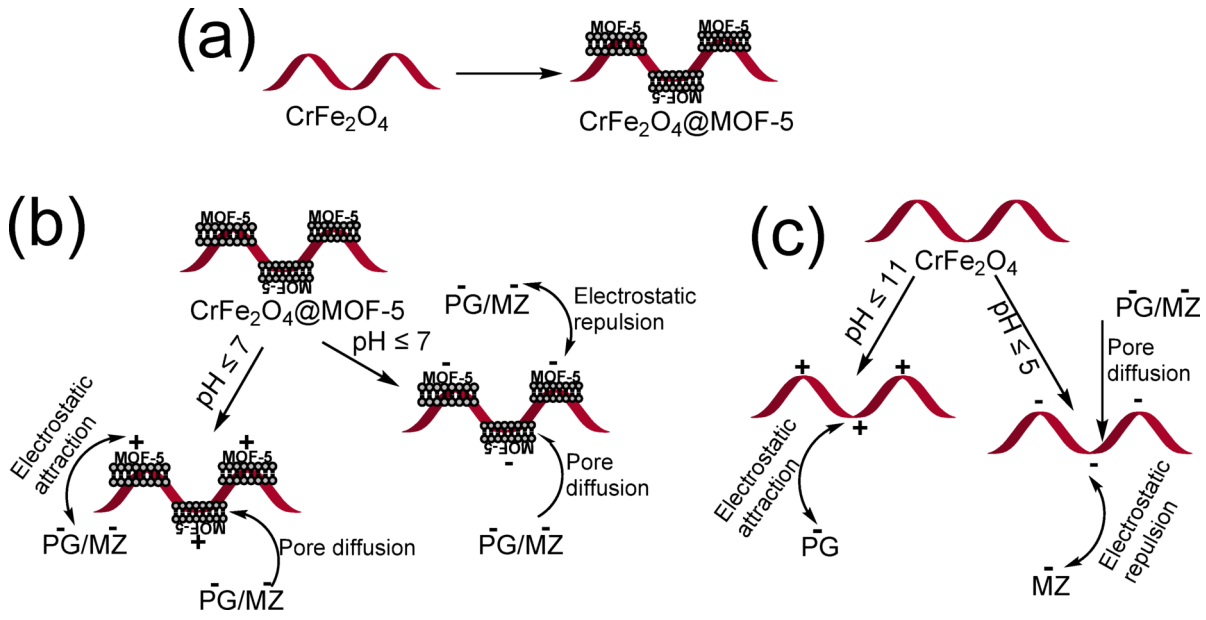


**Fig. 9**. Illustration for the conversion of $CrFe_2O_4$ to $CrFe_2O_4$@MOF-5 (**a**). Mechanism for the removal of PG and MZ by (**b**) $CrFe_2O_4$@MOF-5, mechanism for the removal of PG and MZ by (**c**) $CrFe_2O_4$.

| Model | Parameter | $CrFe_2O_4$ | $CrFe_2O_4$@MOF-5 |
|---|---|---|---|
| MZ | | | |
| Pseudo-1st -order model | $q_e$ (mg $g^{-1}$)<br>$k_1$ ($min^{-1}$)<br>$r^2$ | 55.15<br>$8.7\times10^{-5}$<br>0.91 | 91.01<br>1.972<br>0.98 |
| Pseudo-2nd -order model | qe (mg $g^{-1}$)<br>$k_2$(g $mg^{-1}$ $min^{-1}$)<br>$r^2$ | 119.1<br>1.418<br>0.99 | 119.1<br>1.973<br>0.97 |
| Experimental data | $q_e$ (mg $g^{-1}$) | 50.41 | 90.24 |
| PG | | | |
| Pseudo-1st -order model | $q_e$ (mg $g^{-1}$)<br>$k_1$ ($min^{-1}$)<br>$r^2$ | 83.14<br>$9.01\times10^{-5}$<br>0.90 | 93.37<br>$1.8\times10^{-4}$<br>0.98 |
| Pseudo-2nd -order model | qe (mg $g^{-1}$)<br>$k_2$(g $mg^{-1}$ $min^{-1}$)<br>$r^2$ | 123.53<br>$1.182\times10^{-6}$<br>0.97 | 120.48<br>$1.8\times10^{-4}$<br>0.90 |
| Experimental data | $q_e$ (mg $g^{-1}$) | 53.82 | 91.67 |

**Table 1**. Kinetic parameters for the removal of MZ and PG on adsorbents.

| Isotherm | $CrFe_2O_4$ | $CrFe_2O_4$@MOF-5 |
|---|---|---|
| MZ | | |
| Langmuir model | | |
| $Q_o$ (mg $g^{-1}$) | 54.35 | 185.20 |
| $K_L$ (L $mg^{-1}$) | 0.123 | 0.092 |
| $r^2$ | 0.95 | 0.96 |
| $R_L$ | 0.076 | 0.098 |
| Freundlich model | | |
| $K_f$ (L $mg^{-1}$) | 5.91 | 13.922 |
| 1/n | 1.7334 | 11.76 |
| $r^2$ | 0.99 | 0.97 |
| Temkin model | | |
| A (L/g) | 1.62 | 1.81 |
| B (J $mol^{-1}$) | 18.63 | 27.97 |
| $r^2$ | 0.91 | 0.82 |
| PG | | |
| Langmuir model | | |
| $Q_o$ (mg $g^{-1}$) | 58.14 | 119.05 |
| $K_L$ (L $mg^{-1}$) | 0.395 | 0.122 |
| $r^2$ | 0.96 | 0.95 |
| $R_L$ | 0.025 | 0.076 |
| Freundlich model | | |
| $K_f$ (L $mg^{-1}$) | 9.29 | 17.73 |
| 1/n | 1.832 | 0.84 |
| $r^2$ | 0.90 | 0.97 |
| Temkin model | | |
| A (L/g) | 1.60 | 2.83 |
| B (J $mol^{-1}$) | 19.81 | 50.85 |
| $r^2$ | 0.91 | 0.93 |

**Table 2**. Isotherm parameters for the removal of MZ and PG.

The data obtained were further subjected to isotherm fitting, which covers both Langmuir, Temkin and Freundlich isotherms models. Mathematically, Langmuir isotherm model may be expressed as[59]:

$$\frac{C_e}{q_e} = \frac{1}{Q_o}C_e + \frac{1}{Q_o K_L} \tag{8}$$

The isotherm constant, $K_L$ (L $mg^{-1}$) and maximum monolayer coverage, $Q_o$ (mg $g^{-1}$), were determined by plotting $C_e/q_e$ against $C_e$. The values of $Q_o$ for the sorption of MZ by $CrFe_2O_4$@MOF-5 (185.20 mg $g^{-1}$) are

higher than that of $CrFe_2O_4$ (54.35 mg $g^{-1}$), while in the case of PG, the values are 119.05 and 58.14 mg $g^{-1}$, respectively for $CrFe_2O_4$@MOF-5 and $CrFe_2O_4$. Data were further subjected to Eq. 9, to determine the $R_L$ value by relating RL to energy, $K_L$[60]:

$$R_L = \frac{1}{1 + K_L C_o} \tag{9}$$

The nature of the Langmuir isotherm is related to the sorption process by the value of $R_L$, which is considered as follows: the Langmuir isotherm is favoured when $0 < R_L < 1$ and unfavoured when $R_L > 1$. In situations where $R_L = 1$, sorption is linear and where $R_L = 0$, the sorption process is described as irreversible[60]. The values of $R_L$ are in the range $0 < R_L < 1$, indicating that the Langmuir isotherm is favoured in the sorption of MZ and PG by nanomaterails, which further suggests the sorption process involves a monolayer covering of the surface of $CrFe_2O_4$@MOF-5 and $CrFe_2O_4$ by the molecules of MZ and PG.

The Temkin model is described in a linear form as[61]:

$$q_e = \left(\frac{RT}{b}\right) In\,(AC_e) \tag{10}$$

$$q_e = BInA + BInC_e \tag{11}$$

In Eqs. 10 and 11, T (K) is the absolute temperature, $b$ (J $mol^{-1}$) is the Temkin constant while $R$ (8.314 J $mol^{-1}$ K) represents gas constant. A (L $g^{-1}$) stands for the equilibrium binding constant, B (J $mol^{-1}$) = RT/b. The values of A and B are derivable from the plot of $q_e$ against ln $C_e$ as presented in Table 2. The $r^2$ values obtained are lower than those of Langmuir and Freundlich isotherms for MZ (for both $CrFe_2O_4$ and $CrFe_2O_4$@MOF-5) and PG (except for the Freundlich isotherm in the case of $CrFe_2O_4$). However, the sorption of PG by $CrFe_2O_4$ can be best described by Langmuir isotherm with an $r^1$ value of 0.96 suggesting a monolayer sorption process.

The Freundlich isotherm can be expressed as[62]:

$$q_e = K_F C_e^{1/n} \tag{12}$$

The Freundlich isotherm constants, $K_F$ (L $mg^{-1}$) were obtained by plotting ln $q_e$ against ln $C_e$ for the sorption of MZ and PG by the $CrFe_2O_4$@MOF-5 and $CrFe_2O_4$. Values are presented in Table 2. As previously reported, the process may be expressed in terms of 1/n values[63], suggesting a normal sorption process when $1/n < 1$ and a sorption process independent of antibiotic concentration when 1/n. However, when the value is $1/n > 1$, the sorption process is a coorperative adsorption. In this study, the value of 1/n is > 1, which suggests a cooperative sorption process, except for the sorption of PG by the $CrFe_2O_4$@MOF-5, where the value of 1/n became < 1, which indicates the sorption of PG by the $CrFe_2O_4$@MOF-5, to be a normal sorption process. From the $r^2$ values, which are not less than 0.95, both Freundlich and Langmuir isotherms may describe the sorption of MZ and PG by the $CrFe_2O_4$@MOF-5. On the other hand, sorption of MZ and PG by $CrFe_2O_4$ fitted best for Langmuir isotherm. This suggest that both monolayer and multilayer sorption process were taking place at the same time when $CrFe_2O_4$@MOF-5 sorbed PG and MZ, which is corroborated by the close $r^2$ values obtained in both situations for Langmuir and Freundlich. Such occurrence may be attributed to the functional group (carboxylate moeity and phenylene ring group) present on the surface of $CrFe_2O_4$@MOF-5; furthermore, the heterogeneous surface mophology of $CrFe_2O_4$@MOF-5 as seen in the SEM images must have contributed to multilayer arrangement in which not all the adsorbed molecules of PG or MZ are in direct contact with the surface of $CrFe_2O_4$@MOF-5. In addition, the consistent pattern of arrangement of the irregular shaped particles may have contributed to the monolayer sorption in $CrFe_2O_4$@MOF-5. Similar observation have been previously reported[64–66].

## Process thermodynamic parameters describing the sorption of PG and MZ

The effect of temperature on the adsorption capacity expressed by the $CrFe_2O_4$@MOF-5 and $CrFe_2O_4$ is shown in Fig. 10a and b. The adsorption capacity of $CrFe_2O_4$@MOF-5 and $CrFe_2O_4$ towards MZ and PG increased with temperature. When the temperature increased from 30 to 50°C, the adsorption capacity by $CrFe_2O_4$ towards MZ increased from 50.41 to 77.24 mg $g^{-1}$ (Table 3), while towards PG, it increased from 53.82 to 86.53 mg $g^{-1}$ (Table 4). A similar trend was observed with the $CrFe_2O_4$@MOF-5. The change in the Gibbs free energy (ΔG) was found negative at all temperatures studied for both nanomaterials for removing the antibiotics from the solution. The negative values of ΔG suggest the process to be spontaneous. The change in enthalpy ($\Delta H^o$) and entropy ($\Delta S^o$) were calculated from $q_e$ (mg $g^{-1}$), equilibrium constant ($b_o$), gas constant (R, 8.314 J $mol^{-1}$ $K^{-1}$), temperature (T, kelvin) and $C_e$ (mg $L^{-1}$) as expressed below[62]:

$$b_o = \frac{q_e}{C_e} \tag{13}$$

$$\Delta G^o = -RTInb_o \tag{14}$$

$$\Delta G^o = \Delta H^o - T\Delta S^o \tag{15}$$

The values of $\Delta H^o$ and $\Delta S^o$ were obtained from the plot of ln $bo$ against 1/T. The value of $\Delta S^o$ from the study is positive, as shown in Table 5. Similarly, the values of $\Delta H^o$ are also positive except for the sorption of PG by the $CrFe_2O_4$@MOF-5, which is negative (-19.23 kJ $mol^{-1}K^{-1}$), suggesting the removal to be exothermic. In contrast, the positive values of $\Delta H^o$ suggest an endothermic process.

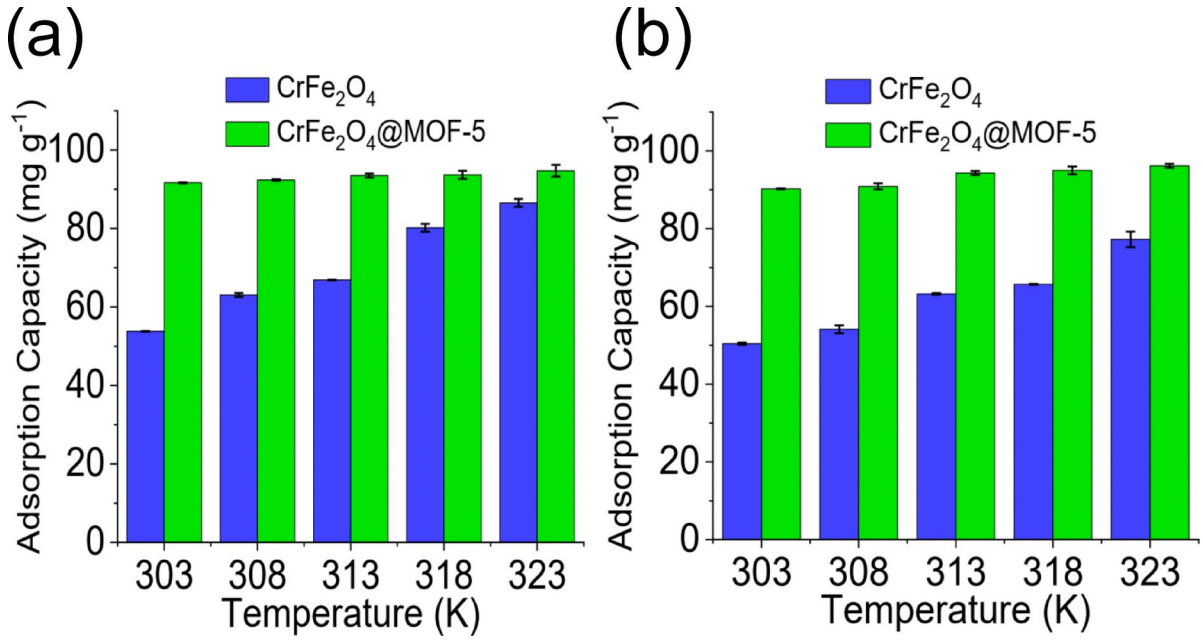


**Fig. 10**. Effect of temperature change on the removal of PG (a) and MZ by $CrFe_2O_4$ and $CrFe_2O_4$@MOF-5.

| $CrFe_2O_4$ | | | | | |
|---|---|---|---|---|---|
| Temperature (K) | 303 | 308 | 313 | 318 | 323 |
| Removal (mg g$^{-1}$) | 50.41 | 54.12 | 63.24 | 65.71 | 77.24 |
| $\Delta G$ (kJ mol$^{-1}$K$^{-1}$) | -2.56 | -3.02 | -4.48 | -5.07 | -9.11 |
| $CrFe_2O_4$@MOF-5 | | | | | |
| Temperature (K) | 303 | 308 | 313 | 318 | 323 |
| Removal (mg g$^{-1}$) | 90.24 | 90.88 | 94.35 | 95.00 | 96.18 |
| $\Delta G$ (kJ mol$^{-1}$K$^{-1}$) | -23.28 | -25.53 | -43.48 | -50.23 | -67.56 |

**Table 3**. Comparison of performance $CrFe_2O_4$ and $CrFe_2O_4$@MOF-5 towards MZ at different temperatures.

| $CrFe_2O_4$ | | | | | |
|---|---|---|---|---|---|
| Temperature (K) | 303 | 308 | 313 | 318 | 323 |
| Removal (mg g$^{-1}$) | 53.82 | 63.06 | 66.88 | 80.21 | 86.53 |
| $\Delta G$ (kJ mol$^{-1}$K$^{-1}$) | -2.94 | -4.37 | -5.25 | -10.71 | -17.24 |
| $CrFe_2O_4$@MOF-5 | | | | | |
| Temperature (K) | 303 | 308 | 313 | 318 | 323 |
| Removal (mg g$^{-1}$) | 91.67 | 92.36 | 93.47 | 93.68 | 94.72 |
| $\Delta G$ (kJ mol$^{-1}$K$^{-1}$) | -27.71 | -30.96 | -37.26 | -39.19 | -48.20 |

**Table 4**. Comparison of performance $CrFe_2O_4$ and $CrFe_2O_4$@MOF-5 towards PG at different temperatures.

## Regeneration of $CrFe_2O_4$@MOF-5 and $CrFe_2O_4$ for reuse

The desorption of MZ and PG from the surfaces of $CrFe_2O_4$@MOF-5 and $CrFe_2O_4$ using different solvents is shown in Fig. 11a and b, which revealed $CH_3OH$ as the best solvent for the desorption process among all the solvents used with a desorption capacity above 90%. Therefore, the regeneration of nanomaterials in multiple cycles was investigated using $CH_3OH$. Results showed that the $CrFe_2O_4$@MOF-5 exhibited a better regeneration performance than the $CrFe_2O_4$ (Fig. 11c and d). Its regeneration capacity was consistent and mantained at above 90% at the 10th cycle. The performance of $CrFe_2O_4$@MOF-5 and $CrFe_2O_4$ was compared with adsorbent from previous research works, as shown in Table 6. The adsorption capacity exhibited by the $CrFe_2O_4$@MOF-5 compares favourably with most adsorbents for removing MZ and PG from the solution. The adsorption capacity of $CrFe_2O_4$@MOF-5 towards PG is higher than the capacities reported for activated carbon[22], CuO nanoparticles[67] and HDTMA-Mt[68]. Similarly, the capacity expressed by the $CrFe_2O_4$@MOF-5 towards MZ

| Parameter | $CrFe_2O_4$ | $CrFe_2O_4$@MOF-5 |
|---|---|---|
| MZ | | |
| $\Delta S^o$ (kJ $mol^{-1}$) | 154.43 | 160.14 |
| $\Delta H^o$ (kJ $mol^{-1}K^{-1}$) | 46.96 | 43.07 |
| PG | | |
| $\Delta S^o$ (kJ $mol^{-1}$) | 229.67 | 83.32 |
| $\Delta H^o$ (kJ $mol^{-1}K^{-1}$) | 69.43 | -19.23 |

**Table 5**. Sorption of MZ and PG thermodynamic parameters.

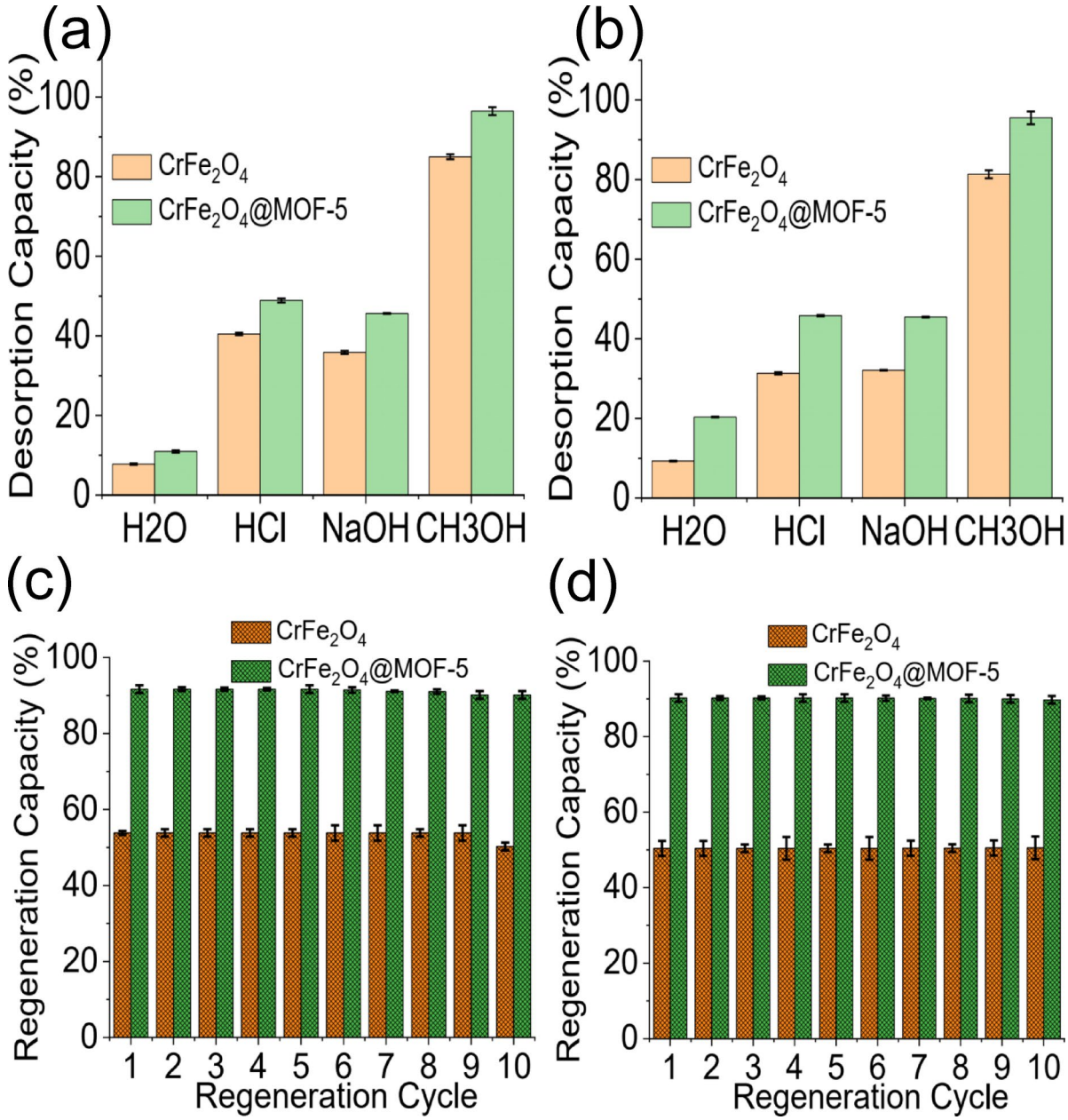


**Fig. 11**. Desorption of PG (**a**) and MZ (**b**) from $CrFe_2O_4$ and $CrFe_2O_4$@MOF-5 and the regeneration capacity by $CrFe_2O_4$ and $CrFe_2O_4$@MOF-5 for PG (**c**) and MZ (**d**).

| Adsorbent | Adsorbate | $Q_o$ (mg $g^{-1}$) | Isotherm | $\Delta G^o_{ads}$ (kJ $mol^{-1}$) | $\Delta H^o_{ads}$ (kJ $mol^{-1}$) | Removal (%) | Desorption (%) | References |
|---|---|---|---|---|---|---|---|---|
| Activated carbon | PG | 8.41 | Langmuir & Freundlich | -58.51 | 55.70 | 69.48 | 32.98 (4th cycle) | 22 |
| CD@MIP | PG | 47.05 | Langmuir | - | - | - | - | 73 |
| MgO | PG | 25.66 | Langmuir & Freundlich | - | - | 80.00 | - | 72 |
| Activated carbon | PG | 6.02 | Langmuir | - | - | - | - | 74 |
| Chitosan | PG | 101.44 | Langmuir | - | 5.69 | - | - | 75 |
| $AgZnFe_2O_4$@Ch | MZ | 65.53 | Langmuir | 0.674 | −0.915 | | 50.00 (4th cycle) | 33 |
| $FeNi_3/SiO_2/CuS$ | MZ | 135.14 | Langmuir | -19.88 | +0.06 | 85.26 | 53.97 (5th cycle) | 71 |
| MAC | MZ | 66.22 | Freundlich | - | - | 95.00 | 73.00 (5th cycle) | 76 |
| PW | MZ | 11.38 | Langmuir | - | +11.69 | 91.00 | - | 77 |
| Co/A@CH | MZ | 35.9 | Freundlich | - | - | 55.00 | - | 78 |
| CS-GO | MZ | 29.76 | Langmuir | - | - | - | - | 70 |
| RHA | MZ | 39.00 | Langmuir | -759.10 | +1.83 | 76.47 | - | 79 |
| PY-PAN | MZ | 63.84 | Freundlich | −7.47 | −37.32 | 89.24 | - | 80 |
| CN-HNT | MZ | 15.80 | Langmuir | - | - | 63.19 | - | 69 |
| GO | MZ | 75.22 | Langmuir | -0.346 | 32.86 | - | - | 81 |
| MCNT | MZ | 4.80 | Freundlich | 122.45 | 59.87 | - | - | 82 |
| Duckweed | PG | 36.18 | Langmuir | - | - | 94.60 | - | 83 |
| HTMA-Mt | PG | 88.5 | Freundlich | 0.54 | 13.09 | - | - | 68 |
| Cu oxide nanoparticles | PG | 15.00 | - | - | - | - | 83.00 | 67 |
| Titanium oxide | PG | 35.58 | Langmuir | - | - | - | - | 84 |
| $CoFe_2O_4$ | MZ<br>PG | 54.35<br>58.14 | Langmuir & Freundlich | -2.56<br>-2.94 | 46.96<br>69.43 | 50.41<br>53.82 | 50.53 (10th cycle)<br>50.28 (10th cycle) | This study |
| $CoFe_2O_4$@MOF-5 | MZ<br>PG | 185.20<br>119.05 | Langmuir & Freundlich | -23.28<br>-27.71 | 43.07<br>-19.23 | 90.24<br>91.67 | 90.00 (10th cycle)<br>90.14 (10th cycle) | This study |

**Table 6**. Juxtaposing the performance of $CrFe_2O_4$ and $CrFe_2O_4$@MOF-5 towards PG and MZ with adsorbents previously published. - = Not reported, MCNT = Multi-Walled Carbon Nanotube, HTMA-Mt = Hexadecyltrimethylammonium bromide modified montmorillonite, CN-HNT = chitosan and halloysite nanotubes, PP-PAN = polyaniline-polypyrrole, Co/A@CH = $CoFe_2O_4$/activated carbon@Chitosan, PW = Plantain wood, RHA = Rice husk ash, GO = Graphene oxide.

is higher than those of CTN-HNT[69], CS-GO[70] and $AgZnFe_2O_4$@Ch[33] except for $FeNi_3/SiO_2/CuS$[71] which exhibited a higher adsorption capacity than $CrFe_2O_4$@MOF-5 for the MZ sorption. The regeneration capacity of $CrFe_2O_4$@MOF-5 is better than most reported adsorbents found in the literature. Moreover, the current study is in accordance with previous studies, which indicated that the sorption process may be described by both Langmuir and Freundlich isotherms[22,72].

## Conclusion

Contamination of water systems by antibiotics such as MZ and PG is a global challenge requiring the development of sustainable solutions for water purification. This study synthesized and compared the capacity of $CrFe_2O_4$@MOF-5 and $CrFe_2O_4$ to remove MZ and PG from water systems. The characterization results showed that both $CrFe_2O_4$@MOF-5 and $CrFe_2O_4$ exhibited a four-phase mass loss from the TGA results, while the BET revealed a surface area of 40.94 $m^2\ g^{-1}$ for $CrFe_2O_4$ and 59.76 $m^2\ g^{-1}$ for $CrFe_2O_4$@MOF-5. The SEM images showed the surfaces of $CrFe_2O_4$@MOF-5 and $CrFe_2O_4$ to be heterogeneous, while EDX confirmed the constituent elements of $CrFe_2O_4$@MOF-5 and $CrFe_2O_4$ to be Cr, Fe, O, C and Zn. In terms of PG adsorption capacity, the $CrFe_2O_4$@MOF-5 exhibited a higher value than the $CrFe_2O_4$ (91.67 vs. 53.82 mg $g^{-1}$). Similarly, the performance of $CrFe_2O_4$@MOF-5 (90.24 mg $g^{-1}$) is better than that of $CrFe_2O_4$ (50.41 mg $g^{-1}$) towards MZ. The Freundlich and Langmuir isotherm may describe the sorption process of MZ and PG by $CrFe_2O_4$@MOF-5 and $CrFe_2O_4$ in an adsorption mechanism that may include electrostatic interaction and pore diffusion. The sorption performance of $CrFe_2O_4$@MOF-5 and regeneration capacity compare favourably with most previously reported adsorbents in literature.

## Data availability

Data will be provided by the corresponding author on request.

Received: 13 December 2024; Accepted: 29 April 2025
Published online: 08 May 2025

## References

1. Derakhshan, Z. et al. Removal methods of antibiotic compounds from aqueous environments–a review. *J. Environ. Health Sustain. Dev.* **1**, 43–62 (2016).

2. Walsh, C. & Wencewicz, T. *Antibiotics: Challenges, Mechanisms, Opportunities* (Wiley, 2020).
3. Adeleke, B. K., Olalekan, O. A., Adewuyi, A., Lau, W. J. & Adeyemi, O. G. Purification of metronidazole and penicillin-G contaminated water by MOF-5 imprinted Cobalt ferrite. *Results Chem.* **6**, 101158 (2023).
4. Francino, M. Antibiotics and the human gut microbiome: Dysbioses and accumulation of resistances. *Front. Microbiol.* **6**, 164577 (2016).
5. Liu, X., Steele, J. C. & Meng, X. Z. Usage, residue, and human health risk of antibiotics in Chinese aquaculture: A review. *Environ. Pollut.* **223**, 161–169 (2017).
6. Chen, J., Ying, G. G. & Deng, W. J. Antibiotic residues in food: Extraction, analysis, and human health concerns. *J. Agric. Food Chem.* **67**, 7569–7586 (2019).
7. O'Neill, J. Tackling drug-resistant infections globally: Final report and recommendations. (2016).
8. Lyu, J., Chen, Y. & Zhang, L. Antibiotics in Drinking Water and Health Risks—China, *China CDC Weekly* **2**, 413 (2020).
9. Tadić, Đ. et al. Occurrence and human health risk assessment of antibiotics and their metabolites in vegetables grown in field-scale agricultural systems. *J. Hazard. Mater.* **401**, 123424 (2021).
10. Khan, S. et al. Investigating the teratogenic potential of diclofenac sodium on chick embryos: A warning for pregnant women. *Toxicol. Rep.* **12**, 292–298 (2024).
11. Sanganyado, E. & Gwenzi, W. Antibiotic resistance in drinking water systems: Occurrence, removal, and human health risks. *Sci. Total Environ.* **669**, 785–797 (2019).
12. Ben, Y. et al. Efficient detection and assessment of human exposure to trace antibiotic residues in drinking water. *Water Res.* **175**, 115699 (2020).
13. de Ilurdoz, M. S., Sadhwani, J. J. & Reboso, J. V. Antibiotic removal processes from water & wastewater for the protection of the aquatic environment-a review. *J. Water Process. Eng.* **45**, 102474 (2022).
14. Tahri, L., Hafiane, F. Z. & Fekhaoui, M. Prevalence and antibiotic resistance of the Escherichia coli in the groundwater (Tadla-Morocco). *Groundw. Sustain. Dev.* **13**, 100572 (2021).
15. Viana, P. et al. Identification of antibiotics in surface-groundwater. A tool towards the ecopharmacovigilance approach: A Portuguese case-study. *Antibiotics* **10**, 888 (2021).
16. Guan YiDong, G. Y. et al. Occurrence and fate of antibiotics in the aqueous environment and their removal by constructed wetlands in China: A review. (2017).
17. Nasrollahi, N., Vatanpour, V. & Khataee, A. Removal of antibiotics from wastewaters by membrane technology: limitations, successes, and future improvements. *Sci. Total Environ.* **838**, 156010 (2022).
18. Yan, F., An, L., Xu, X., Du, W. & Dai, R. A review of antibiotics in surface water and their removal by advanced electrocoagulation technologies. *Sci. Total Environ.* **906**, 167737 (2024).
19. Phoon, B. L. et al. Conventional and emerging technologies for removal of antibiotics from wastewater. *J. Hazard. Mater.* **400**, 122961 (2020).
20. Yang, Q. et al. Antibiotics: an overview on the environmental occurrence, toxicity, degradation, and removal methods. *Bioengineered* **12**, 7376–7416 (2021).
21. Mahmud, F. et al. Antibiotic-contaminated wastewater treatment and remediation by electro-advanced oxidation processes (EAOPs). *Groundw. Sustain. Dev.*, 101181 (2024).
22. Pouretedal, H. & Sadegh, N. Effective removal of amoxicillin, cephalexin, Tetracycline and penicillin G from aqueous solutions using activated carbon nanoparticles prepared from vine wood. *J. Water Process. Eng.* **1**, 64–73 (2014).
23. Adewuyi, A. & Oderinde, R. A. Graphitic carbon nitride-modified cerium ferrite: An efficient photocatalyst for the degradation of Ciprofloxacin, ampicillin, and erythromycin in aqueous solution. *J. Mater. Sci. Mater. Eng.* **19**, 37 (2024).
24. Gujarathi, N. P. *Phytoremediation of Tetracycline and Oxytetracycline* (Colorado State University, 2005).
25. Wang, J. et al. Performance and mechanism of removal of antibiotics and antibiotic resistance genes from wastewater by electrochemical carbon nanotube membranes. *Front. Chem.* **10**, 973490 (2022).
26. Javed, M. S. et al. Advanced materials for photocatalytic removal of antibiotics from wastewater. *J. Alloys Compd.*, **177926** (2024).
27. Shen, Y., Fang, Q. & Chen, B. Environmental applications of three-dimensional graphene-based macrostructures: Adsorption, transformation, and detection. *Environ. Sci. Technol.* **49**, 67–84 (2015).
28. Nag, S. et al. Strategic optimization of phase-selective thermochemically amended terra-firma originating from excavation-squander for Geogenic fluoride adsorption: a combined experimental and in Silico approach. *Environ. Sci. Pollut. Res.* **29**, 77821–77838 (2022).
29. Pal, R. et al. Real time monitoring of heavy metal adulteration in biodiesel using arduino UNO Platform@ A promising multi-purpose stimuli-responsive azomethine based chemoreceptor for hierarchical tri-ionic sensing. *Microchem. J.* **207**, 111739 (2024).
30. Eleryan, A. et al. Isothermal and kinetic screening of Methyl red and Methyl orange dyes adsorption from water by Delonix regia biochar-sulfur oxide (DRB-SO). *Sci. Rep.* **14**, 13585 (2024).
31. Nazir, M. A. et al. Heterointerface engineering of water stable ZIF-8@ ZIF-67: Adsorption of Rhodamine B from water. *Surf. Interfaces*. **34**, 102324 (2022).
32. Nazir, M. A. et al. Synthesis of bimetallic Mn@ ZIF–8 nanostructure for the adsorption removal of Methyl orange dye from water. *Inorg. Chem. Commun.* **165**, 112294 (2024).
33. Rajabi, S. et al. Metronidazole adsorption by bio-synthesized silver-zinc ferrite nanoadsorbent in presence of Chitosan from aqueous media: Response surface methodology. *Appl. Water Sci.* **14**, 92 (2024).
34. Venugopalan, P. L., Jain, S., Shivashankar, S. & Ghosh, A. Single coating of zinc ferrite renders magnetic nanomotors therapeutic and stable against agglomeration. *Nanoscale* **10**, 2327–2332 (2018).
35. Abbas, S. et al. Cutting-edge metal-organic frameworks: Revolutionizing the adsorptive removal of pharmaceutical contaminants from water. *Rev. Inorg. Chem.* (2025).
36. Ul Khair, K. et al. Mercury removal from water: Insights from MOFs and their composites. *Rev. Inorg. Chem.* **44**, 671–684 (2024).
37. Khan, N. A. et al. Development of Mn-PBA on GO sheets for adsorptive removal of Ciprofloxacin from water: Kinetics, isothermal, thermodynamic and mechanistic studies. *Mater. Chem. Phys.* **245**, 122737 (2020).
38. Ahmad, K. et al. Engineering of zirconium based metal-organic frameworks (Zr-MOFs) as efficient adsorbents. *Mater. Sci. Eng. B.* **262**, 114766 (2020).
39. Xie, D. et al. Facile synthesis of Cr-doped ferrite catalyst from Cr-containing electroplating sludge with activated persulfate for efficient degradation of Tetracycline. *J. Environ. Chem. Eng.* **10**, 108805 (2022).
40. Spivakov, A. A., Huang, L. H., Chen, Y. Z. & Lin, C. R. Facile synthesis of Chromium-Doped Fe1. 1Mn1. 9O4 nanoparticles and the effect of cr content on their magnetic and structural properties. *Nanomaterials* **13**, 2203 (2023).
41. Kuznetsov, M., Pankhurst, Q. & Parkin, I. Self propagating high-temperature synthesis of chromium substituted magnesium zinc ferrites Mg 0.5 Zn 0.5 Fe 2–x cr X O 4 ($0 \le x \le 1.5$). *J. Mater. Chem.* **8**, 2701–2706 (1998).
42. Adewuyi, A. Chemically modified biosorbents and their role in the removal of emerging pharmaceutical waste in the water system. *Water* **12**, 1551 (2020).
43. Adewuyi, A. Ferrite doped metal–organic framework: Novel material for photocatalytic degradation of antibiotics in the polluted water system–A review. *Environ. Nanatechnol. Monit. Manag.* **20**, 100829 (2023).
44. Firouzjaei, M. D. et al. Exploiting synergetic effects of graphene oxide and a silver-based metal–organic framework to enhance antifouling and anti-biofouling properties of thin-film nanocomposite membranes. *ACS Appl. Mater. Interfaces.* **10**, 42967–42978 (2018).

45. Kumar, G. & Masram, D. T. Sustainable synthesis of MOF-5@ GO nanocomposites for efficient removal of Rhodamine B from water. *ACS Omega*. **6**, 9587–9599 (2021).
46. Adewuyi, A. et al. Use of Urea-imprinted Cobalt ferrite nanoparticles in deacidification of deteriorated vegetable oil: Synthesis, characterization and preclinical toxicity screening. *J. Mol. Liq.* **365**, 120224 (2022).
47. Adewuyi, A. & Oderinde, R. A. Tartaric acid-modified CuFe2O4: Potential application in the purification of butylated hydroxyanisole and butylated hydroxytoluene-contaminated water. *J. Mater. Res.* **37**, 3033–3048 (2022).
48. Asadevi, H. et al. ZnO@ MOF-5 as a fluorescence Turn-Off sensor for ultrasensitive detection as well as probing of copper (II) ions. *ACS Omega*. **7**, 13031–13041 (2022).
49. Sivakumar, P., Ramesh, R., Ramanand, A., Ponnusamy, S. & Muthamizhchelvan, C. Synthesis, studies and growth mechanism of ferromagnetic $NiFe_2O_4$ nanosheet. *Appl. Surf. Sci.* **258**, 6648–6652 (2012).
50. Sivakumar, P., Ramesh, R., Ramanand, A., Ponnusamy, S. & Muthamizhchelvan, C. Synthesis and characterization of $NiFe_2O_4$ nanosheet via polymer assisted co-precipitation method. *Mater. Lett.* **65**, 483–485 (2011).
51. Tirmizi, S. A. et al. Synthesis of highly stable MOF-5@ MWCNTs nanocomposite with improved hydrophobic properties. *Arab. J. Chem.* **11**, 26–33 (2018).
52. Chen, G. et al. Investigation of metal-organic framework-5 (MOF-5) as an antitumor drug Oridonin sustained release carrier. *Molecules* **24**, 3369 (2019).
53. Zhu, L. et al. Structure and adsorptive desulfurization performance of the composite material MOF-5@ AC. *New J. Chem.* **42**, 3840–3850 (2018).
54. Gangu, K. K., Maddila, S. & Jonnalagadda, S. B. The pioneering role of metal–organic framework-5 in ever-growing contemporary applications–a review. *RSC Adv.* **12**, 14282–14298 (2022).
55. Yurdakal, S., Garlisi, C., Özcan, L., Bellardita, M. & Palmisano, G. *In Heterogeneous Photocatalysis* 87–152 (Elsevier, 2019).
56. Tian, L., Zhang, J., Shi, H., Li, N. & Ping, Q. Adsorption of malachite green by diatomite: Equilibrium isotherms and kinetic studies. *J. Dispers. Sci. Technol.* **37**, 1059–1066 (2016).
57. Adewuyi, A., Gervasi, C. A. & Mirífico, M. V. Synthesis of strontium ferrite and its role in the removal of Methyl orange, phenolphthalein and bromothymol blue from laboratory wastewater. *Surf. Interfaces*. **27**, 101567 (2021).
58. Olalekan, O. A., Campbell, A. J., Adewuyi, A., Lau, W. J. & Adeyemi, O. G. Synthesis and application of ZnO-MgO-NiO@ stearicamide mixed oxide for removal of Ciprofloxacin and ampicillin from aqueous solution. *Results Chem.* **4**, 100457 (2022).
59. Muraina, T. A., Olalekan, O. A., Adewuyi, A. & Adeyemi, O. G. Preparation and application of nickel copper ferrate and its metal–organic framework composite in the decontamination of chemical indicator contaminated synthetic and Raw laboratory wastewater. *Results Chem.* **6**, 101142 (2023).
60. Adewuyi, A. & Oderinde, R. A. Chemically modified vermiculite clay: a means to remove emerging contaminant from polluted water system in developing Nation. *Polym. Bull.* **76**, 4967–4989 (2019).
61. Ushedo, T. R., Adeyemi, O. G., Adewuyi, A. & Lau, W. J. Synthesis of N, N (1, 3-phenylene) dimethanimine: A useful resource for the removal of free fatty acid in waste vegetable oil. *Sci. Afr.* **16**, e01188 (2022).
62. Campbell, A. J. et al. Synthesis and application of $SeFe_2O_4$@ cell for the removal of polyethylene glycol from aqueous solution. *Environ. Nanatechnol. Monit. Manag.* **20**, 100802 (2023).
63. Adewuyi, A. & Pereira, F. V. Preparation and application of EDTA-functionalized underutilized Adansonia digitata seed for removal of Cu (II) from aqueous solution. *Sustain. Environ. Res.* **28**, 111–120 (2018).
64. Chairat, M., Rattanaphani, S., Bremner, J. B. & Rattanaphani, V. An adsorption and kinetic study of Lac dyeing on silk. *Dyes Pigm.* **64**, 231–241 (2005).
65. Dang Son, B. H., Mai, Q., Xuan Du, V. & Hai Phong, D. N. & Quang Khieu, D. A study on astrazon black AFDL dye adsorption onto Vietnamese diatomite. *J. Chem.* 8685437 (2016).
66. Othman, N. H. et al. Adsorption kinetics of methylene blue dyes onto magnetic graphene oxide. *J. Environ. Chem. Eng.* **6**, 2803–2811 (2018).
67. Ahmadi, S. & Adaobi Igwegbe, C. Kinetic studies on penicillin G removal from aqueous environments by cupric oxide nanoparticles. *Arch. Hyg. Sci.* **10**, 86–96 (2021).
68. Nourmoradi, H., Daneshfar, A., Mazloomi, S., Bagheri, J. & Barati, S. Removal of penicillin G from aqueous solutions by a cationic surfactant modified montmorillonite. *MethodsX* **6**, 1967–1973 (2019).
69. Açıkel, Y. S. Investigation of adsorption of metronidazole on Chitosan-Halloysite nanocomposites and controlled release. *Indian J. Chem. Technol. (IJCT)*. **27**, 101–115 (2020).
70. Parashar, D., Harafan, A., Achari, G. & Kumar, M. Ciprofloxacin and metronidazole adsorption on chitosan-modified graphene oxide as single-compound and binary mixtures: Kinetics, isotherm, and sorption mechanism. *J. Hazard. Toxic. Radioact. Waste.* **27**, 04022042 (2023).
71. Nasseh, N., Barikbin, B., Taghavi, L. & Nasseri, M. A. Adsorption of metronidazole antibiotic using a new magnetic nanocomposite from simulated wastewater (isotherm, kinetic and thermodynamic studies). *Compos. Part. B Eng.* **159**, 146–156 (2019).
72. Rahdar, S., Rahdar, A., Khodadadi, M. & Ahmadi, S. Error analysis of adsorption isotherm models for penicillin G onto magnesium oxide nanoparticles. *Appl. Water Sci.* **9**, 1–7 (2019).
73. Xu, Y. et al. Selective adsorption and identification of penicillin G sodium in milk by molecularly imprinted polymer doped carbon Dot. *Microchim. Acta*. **191**, 186 (2024).
74. Bouhcain, B. et al. in *AIP Conference Proceedings*. (AIP Publishing).
75. Masoudi, F., Kamranifar, M. & Naghizadeh, A. The efficiency of Chitosan extracted from Persian Gulf shrimp shell in removal of penicillin G antibiotic from aqueous environment. *Iran. J. Chem. Chem. Eng.* **39**, 235–244 (2020).
76. Ahmadfazeli, A. et al. Removal of metronidazole antibiotic from aqueous solution by ammonia-modified activated carbon: Adsorption isotherm and kinetic study. *J. Water Sanitation Hyg. Dev.* **11**, 1083–1096 (2021).
77. Amouei, A., Naghipour, D., Taghavi, K. & Estaji, M. Removal of metronidazole antibiotic from hospital wastewater by biosorbent prepared from plantain wood. *J. Babol Univ. Med. Sci.* **22** (2020).
78. Malakootian, M., Nasiri, A. & Mahdizadeh, H. Metronidazole adsorption on $CoFe_2O_4$/Activated Carbon@ Chitosan as a new magnetic biocomposite: Modelling, analysis, and optimization by response surface methodology. (2019).
79. Abbas, H. & Abbas, A. S. Adsorption of Flagyl on prepared Ash from rice husk. *Iraqi J. Chem. Pet. Eng.* **22**, 11–17 (2021).
80. Aarab, N. et al. Removal of an emerging pharmaceutical pollutant (metronidazole) using PPY-PANi copolymer: Kinetics, equilibrium and DFT identification of adsorption mechanism. *Groundw. Sustain. Dev.* **11**, 100416 (2020).
81. Balarak, D., Mostafapour, F., Azarpira, H. & Joghataei, A. Mechanisms and equilibrium studies of sorption of metronidazole using graphene oxide. *J. Pharm. Res. Int.* **19**, 1–9 (2017).
82. Kariim, I., Abdulkareem, A. & Abubakre, O. Development and characterization of MWCNTs from activated carbon as adsorbent for metronidazole and Levofloxacin sorption from pharmaceutical wastewater: Kinetics, isotherms and thermodynamic studies. *Sci. Afr.* **7**, e00242 (2020).
83. Balarak, D., Mostafapour, F. & Joghataei, A. Experimental and kinetic studies on penicillin G adsorption by Lemna minor. *Br. J. Pharm. Res.* **9**, 1–10 (2016).
84. Meksi, M. & Kochkar, H. Penicillin G adsorption isotherms and kinetic studies using $TiO_2$ nanotubes free and modified with β-cyclodextrin. *Chem. Lett.* **44**, 1289–1291 (2015).

## Acknowledgements
The authors appreciate the support from the Department of Chemistry, University of Cambridge, UK.

## Author contributions
Adewale Adewuyi: Conceptualization, Formal analysis, Investigation, Writing - Original Draft, Writing – Review and Editing, Visualization. Olalere G Adeyemi: Conceptualization, Formal analysis, Investigation, Writing - Original Draft, Writing – Review and Editing. Woei Jye Lau: Formal analysis, Investigation, Writing - Original Draft, Writing – Review and Editing, Visualization. Babatunde K Adeleke: Investigation, Visualization and Formal analysis. Olamide A Olalekan: Investigation and Formal analysis.

## Declarations

## Competing interests
The authors declare no competing interests.

## Additional information
**Correspondence** and requests for materials should be addressed to A.A.

**Reprints and permissions information** is available at www.nature.com/reprints.

**Publisher's note** Springer Nature remains neutral with regard to jurisdictional claims in published maps and institutional affiliations.